Solid-State Electronics, 1978, Vol. 21, pp. 345–355. Pergamon Press. Printed in Great Britain

A CHARGE-SHEET MODEL OF THE MOSFET

J. R. BREWS
Bell Laboratories, Murray Hill, NJ 07974, U.S.A.

(*Received* 7 *May* 1977; *in revised form* 9 *June* 1977)

Abstract—Intuition, device evolution, and even efficient computation require simple MOSFET (metal-oxide-semiconductor field-effect transistor) models. Among these simple models are charge-sheet models which compress the inversion layer into a conducting plane of zero thickness. It is the purpose of this paper to test one such charge sheet model to see whether this approximation is too severe. This particular model includes diffusion which is expected to be important in the subthreshold and saturation regions.

As a test the charge sheet model is applied to long-channel devices. Long-channel MOSFET behavior has been thoroughly studied, and is very well explained by the Pao–Sah double-integral formula for the current. Hence, a clear-cut test is a comparison of the charge sheet model with the Pao–Sah model.

We find the charge sheet model has two advantages over the Pao-Sah model.

(1) It leads to a very simple algebraic formula for the current of long-channel devices. The same formula applies in all regimes from subthreshold to saturation. Neither splicing nor parameter changes are needed. No discontinuities occur in either the current or the small-signal parameters, or in the derivatives of the small-signal parameters.

(2) It is simpler to extend the charge sheet model to two or three dimensions than the Pao–Sah model. This simplification is a result of dropping the details of the inversion layer charge distribution.

An important aspect of the gradual channel approximation is brought out by the analysis. Suppose the boundary condition relating the quasi-fermi level at the drain, ϕ_{fL}, to that at the source, ϕ_{fo}, namely

$$\phi_{fL} = \phi_{fo} + V_D \tag{1}$$

where V_D is the drain voltage, is applied in all bias regimes. Then it is shown that this means the potential at the drain end of the channel, ϕ_{sL} is *not* related to the potential at the source end of the channel, ϕ_{so}, by

$$\phi_{sL} = \phi_{so} + V_D. \tag{2}$$

Instead, ϕ_{sL} is computed, not imposed as a boundary condition. It is suggested that this failure of the potential to satisfy the boundary condition at the drain is justifiable. That is, ϕ_{sL} should be reinterpreted as the potential at the point in the channel where the gradual channel approximation fails. Hence, (2) may be relaxed. However, the "channel length" in the gradual-channel approximation now becomes a fitting parameter and is not the metallurgical source-to-drain separation.

In addition several aspects of the long-channel MOSFET are brought out: (1) Pinch-off is achieved only asymptotically as the drain voltage tends to infinity. This is in marked contrast to the often-stated, textbook view that pinch-off is achieved for some finite drain voltage, the saturation voltage. (2) The channel or drain conductance approaches zero only asymptotically. (3) The transconductance saturates only asymptotically.

Figures comparing the simple charge-sheet model formulas with the usual textbook formulas are included for direct-current vs drain voltage, channel conductance vs drain voltage, and transconductance vs drain voltage. The charge-sheet model agrees with the original Pao–Sah double-integral formula for the current at all gate and drain voltages, and possesses the correct subthreshold behavior. The textbook formulas do not.

INTRODUCTION

MOSFET theory is undergoing new scrutiny. This new interest is due in part to short channel devices which emphasize two-dimensional effects and, in part, to low voltage operation which emphasizes the near-threshold regime of gate biases.

While full scale numerical attacks on MOSFET theory have been made[1–3], intuition and efficient computation depend upon the establishment of simpler models. Among these simpler models is the class of *charge sheet* models. In these models the inversion layer is compressed into a conducting sheet of zero thickness. The conductivity of this sheet is controlled by the carrier density per unit area in the sheet. However, all detail of the actual charge distribution in the direction normal to the sheet is lost.

A number of such charge sheet models have been proposed. One of the first was that of Guerst[4] which included a number of additional simplifications such as neglect of dopant ions, fixed depletion width, and neglect of diffusion. A more recent and more complete model was proposed by Loeb, Andrew and Love[5], and further explored by Armstrong, Magowan and Ryan[6]. This model included dopant ions, depletion width variations and a two-dimensional potential calculation. However, diffusion was neglected again. Diffusion is known to be significant near saturation and near threshold.

Our purpose here is to test a variation of the charge sheet model of Loeb *et al.*[5] which includes diffusion. As a test the model is applied to long-channel devices and compared with the customary Pao–Sah model[7],

and with various text book formulas[8–10].† These approximate formulas were introduced by Sah and Pao[11] as improvements upon similar formulas derived in a somewhat heuristic manner by Ihantolla and Moll[12] and even earlier in unpublished work by Kahng[13].

The purpose behind this comparison of models is to check whether the charge sheet approximation is so severe as to preclude accurate prediction of MOSFET characteristics. Comparison of the charge-sheet model with the Pao–Sah model has the force of comparison with experiment, since the Pao–Sah model is known to work well for long channel devices.‡

Besides validating the charge-sheet model for long-channel devices, we find the model analysis brings out several features of the long-channel MOSFET not previously recognized.

(1) The saturation of the drain current with increasing drain voltage is *asymptotic*. That is, pinch-off is not reached at any drain voltage less than infinity.

(2) The drain conductance approaches zero only asymptotically, and is never zero for any finite drain voltage.

(3) The transconductance saturates only asymptotically with drain voltage.

These features of the charge sheet model are shared by the Pao–Sah double-integral formulation[7], but were not pointed out by these authors. What is more, simple formulas, such as those introduced by Sah and Pao[11] and used in textbooks[8–10] very explicitly employ a view of saturation contrary to (1) and (2) above.

We find very close agreement between the original Pao–Sah double-integral formula and our charge-sheet model. What is more:

(1) *Simple* formulas for the current, channel conductance, and transconductance are obtained which are valid for all gate and drain voltages. Therefore the cumbersome Pao–Sah formula can be avoided altogether.

(2) Shape variations of the inversion layer are expected because of variations along the channel of the carrier density and normal electric field. These variations are neglected in the charge sheet model, but are included in the Pao–Sah model. Agreement of the two models shows that such variations in the shape of the inversion layer along the channel are unimportant to correct current vs drain voltage characteristics.

(3) Inclusion of diffusion is shown to be necessary in any charge sheet model. Diffusion is needed to obtain correct near-threshold behavior. In addition diffusion is needed to obtain the asymptotic behavior of the channel conductance and transconductance for drain voltages approaching saturation.

In the following discussion we presume that the Pao–Sah model in the double-integral form proposed in Ref. [7] is in excellent agreement with experiment. This double-integral model is referred to as the "Pao–Sah model" here. The term "Sah–Pao approximation" refers to the simple textbook formulas introduced by Sah and Pao in Ref.[11] as approximations to the more basic model of Ref. [7]. For gate voltages well above threshold the error in these formulas is slight[7, 11]. See particularly Fig. 3 in Ref. [7].

FORMULATION OF MODEL

Assuming a quasi-fermi level formulation for carrier densities and the coordinate system of Fig. 1 the source-to-drain current, I, can be related to the average quasi-fermi level gradient, $d\bar{\phi}_f/dy$, and the carrier density per unit area, $N(y)$ by (see Appendix 1)

$$I = Zq\mu^* N(y)\, d\bar{\phi}_f/dy \tag{1}$$

where Z = channel width, μ^* = effective mobility, and "y" measures distance along the channel from the source toward the drain. In Appendix 1 it is shown that (1) is general enough to include even two dimensional current flows. Precise definitions of $d\bar{\phi}_f/dy$ and $N(y)$ have been given in Appendix 1. These definitions are not essential here because we intend simply to approximate $d\bar{\phi}_f/dy$ by

$$\frac{d\bar{\phi}_f}{dy} = \frac{d\phi_s}{dy} - \frac{1}{\beta}\frac{d \ln N}{dy} \tag{2}$$

where $\phi_s(y)$ = potential along oxide-silicon surface and $\beta = q/(kT)$. Equation (2) differs from the model of Refs. [5, 6] in the addition of the second term, which is intended to account for diffusion. Justification of (2) is based upon its success in producing "correct" I–V curves.§ In particular, we show eqn (2) leads to equations only negligibly different from the Pao–Sah model[7] in the case of long-channel MOSFETs. The Pao–Sah model is known to agree with experiment[7, 11]. Integration of (2) provides

$$N(y) = N(o) \exp\{\beta[\phi_s(y) - \phi_s(o)] - \beta[\bar{\phi}_f(y) - \bar{\phi}_f(o)]\}. \tag{3}$$

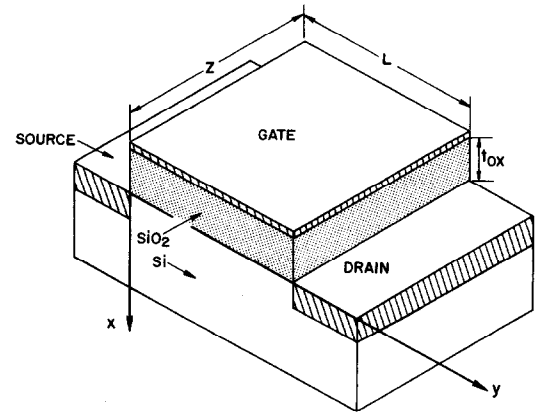

Fig. 1. The coordinate system used for the MOSFET. The channel width is Z, the channel length is L.

†In Ref. [10] see particularly Chap. 10, Section 4.

‡At large gate voltages even the Pao–Sah model does require an empirical mobility adjustment for the Schrieffer effect. This will be true for the charge-sheet model as well. See Ref. [11].

§A "derivation" of (2) can be based upon the usual formula for the electrochemical potential as $\bar{\phi}_f = \bar{\phi}_{fo} - (1/\beta)\ln(N/N_0) + \phi_s - \phi_{so}$, where N_o is the carrier density in the uniform, homogeneous reference state for which $\bar{\phi}_f$ is ϕ_{fo} and the electrical potential everywhere along the interface is ϕ_{so}.

That is, (2) is equivalent to the assumption that the carrier density along the channel varies only because the inversion layer moves rigidly with respect to the quasi-fermi level as the potential varies. All shape dependence of the inversion layer upon carrier density or normal field is contained in $N(o)$ and remains unaltered from source to drain.

If eqn (2) is substituted in (1) we can solve (1) for $N(y)$ to find

$$N(y) = N(o)\exp\{\beta[\phi_s(y) - \phi_s(o)]\} - \frac{I}{kT\mu^* Z} e^{\beta\phi_s(y)} \int_0^y dy_0\, e^{-\beta\phi_s(y_0)}. \quad (4)$$

The model is then completed using Poisson's equation for the potential,

$$\nabla^2\phi = 0 \text{ (in gate oxide)} \quad (5a)$$

$$\nabla^2\phi = -q(p - N_A)/(\kappa\epsilon_0) \text{ (in silicon)} \quad (5b)$$

where we have assumed p-type material. Equations (5a) and (5b) are joined across the oxide-silicon interface by the discontinuity condition

$$\kappa_{ox}\epsilon_o \left.\frac{\partial\phi}{\partial x}\right|_{o^-} - \kappa_{sc}\epsilon_o \left.\frac{\partial\phi}{\partial x}\right|_{o^+} = -qN(y) \quad (6)$$

where (o^-) refers to evaluation on the oxide side of the interface, (o^+) on the silicon side. The x-coordinate measures distance normal to this interface into the silicon. The use of (6) implies $N(y)$ is contained in a charge sheet of zero thickness. This in turn means (i) the current is constrained to flow along the oxide-silicon interface, and (ii) there is no voltage drop across the inversion layer.

Using some arbitrary $\phi_s(y) \equiv \phi(x = 0, y)$ we can solve (5) for ϕ in both oxide and semiconductor. This determines the normal derivatives in (6). Using (4) we obtain an integral equation for $\phi_s(y)$. This equation now will be set up and solved for long channel devices.

LONG-CHANNEL SIMPLIFICATION

For long channel devices it is customarily assumed that Poisson's equation becomes only one dimensional because the potential variations along the channel are gradual compared to those normal to the channel. This is probably accurate not too close to the drain for devices whose channel length, L, greatly exceeds the oxide thickness and depletion depth. Following this procedure, also a feature of the Pao–Sah model [7], we find the field on the semiconductor side of the interface is given by the depletion layer charge:

$$\kappa_{sc}\epsilon_o \left.\frac{d\phi}{dx}\right|_{o^+} = -qN_A L_B \sqrt{[2(\beta\phi_s - 1)]}. \quad (8)$$

Here L_B is the bulk Debye length, $L_B = (kT\kappa_{sc}\epsilon_0/q^2 N_A)^{1/2}$. The y-dependence of ϕ_s is not indicated explicitly. In the oxide the field is constant and given by:

$$\kappa_{ox}\epsilon_o \left.\frac{d\phi}{dx}\right|_{o^-} = -C_{ox}(V_g - \phi_s) \quad (9)$$

where the oxide capacitance per unit area is C_{ox}, $C_{ox} \equiv \kappa_{ox}\epsilon_o/t_{ox}$, t_{ox} = oxide thickness. Substituting (8) and (9) into (6) we obtain:

$$C_{ox}[V_G - \phi_s(y)] = qN_A L_B\{2[\beta\phi_s(y) - 1]\}^{1/2} + qN(y). \quad (10)$$

All fixed-charge and work function effects have been ignored, but their effect is similar to an addition to V_G. If $qN(y)$ is replaced in (10) by the expression (4), then (10) becomes an integral equation for $\phi_s(y)$. This integral equation is solved by a trick. Differentiate (10) with respect to "y". Use (4) in the result to eliminate $dN(y)/dy$:

$$\frac{dN}{dy} = \beta N(y)\frac{d\phi_s}{dy} - \frac{I}{kT\mu^* Z}$$

which will be recognized as a rearrangement of the usual expression for the current as the sum of drift and diffusion components. Now $N(y)$ is eliminated using (10) again. The result is then integrable. Integrating from $y = o$ (the source) to an arbitrary point, y, we find

$$I = \frac{1}{\beta}\mu^*\left(\frac{Z}{y}\right)\{C_{ox}(1 + \beta V_G)(\phi_s - \phi_{so}) - \frac{\beta}{2}C_{ox}(\phi_s^2 - \phi_{so}^2) - qN_A L_B\left(\frac{2\sqrt{2}}{3}\right)[(\beta\phi_s - 1)^{3/2} - (\beta\phi_{so} - 1)^{3/2}] + qN_A L_B\sqrt{(2)}[(\beta\phi_s - 1)^{1/2} - (\beta\phi_{so} - 1)^{1/2}]\} \quad (11)$$

where $\phi_s \equiv \phi_s(y)$ and $\phi_{so} \equiv \phi_s(o)$.

BOUNDARY CONDITIONS

Before employing (11) we must know the value of ϕ_{so} and $\phi_{sL} \equiv \phi_s(y = L)$ for a given gate voltage, V_G, and drain voltage, V_D. First consider ϕ_{so}, the potential at the source end of the channel.

Frequently the approximation is made that $\phi_{so} \approx 2\phi_B$, the nominal threshold condition for the MOSFET. However, this assumption is made neither in the Pao–Sah model nor in the present charge sheet model. Instead, we are free to adopt the same procedure to determine ϕ_{so} in both models. That is, we take ϕ_{so} from the one-dimensional Poisson equation for zero drain voltage, viz.:†

$$C_{ox}(V_G - \phi_{so}) = qN_A L_B\sqrt{(2)}\left[\beta\phi_{so} - 1 + \left(\frac{n_i}{N_A}\right)^2 e^{\beta\phi_{so}}\right]^{1/2} \quad (12)$$

where we assume $(\beta\phi_{so} - 1) \gg \exp(-\beta\phi_{so})$.

For illustration (12) is plotted in Fig. 2. The curves in

†For example, see Ref. [10], p. 431, eqn (11).

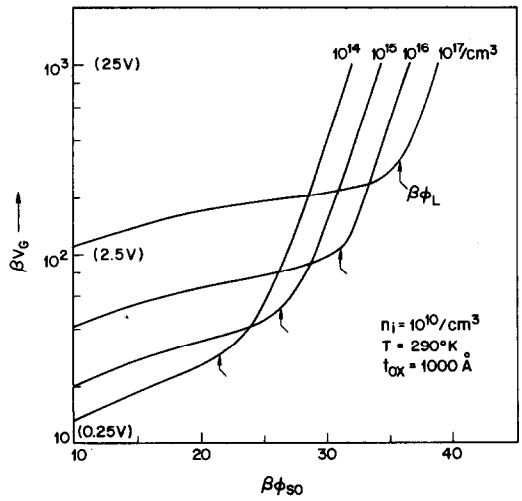

Fig. 2. Potential at the source, ϕ_{so}, as a function of gate voltage, V_G, for various doping levels. The oxide thickness is assumed to be 1000 Å, and we take $n_i = 1 \times 10^{10}/\text{cm}^3$ at 290°K.

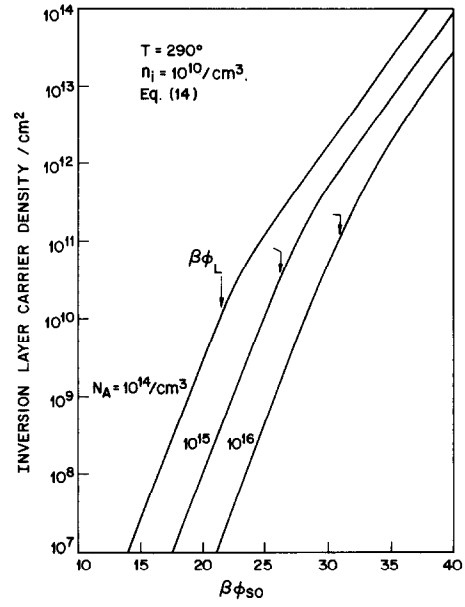

Fig. 3. The carrier density per cm^2 at the source, $N(o)$, vs the potential at the source, ϕ_{so}. The Lindner potential, ϕ_L, is indicated to show the onset of strong inversion.

Fig. 2 were obtained by assuming ϕ_{so} and calculating V_G, which is simpler than the reverse procedure. However if one wishes to find ϕ_{so} for a given V_G, then (12) can be rearranged to provide an algorithm for ϕ_{so}. That is, we use an iterative form of (12):

$$\beta\phi_{so}^{i+1} = \beta\phi_{so}^{o} + \ln\{[\beta(V_G - \phi_{so}^{i})]^2 / [1 + (\beta\phi_{so}^{i} - 1)/\exp\beta(\phi_{so}^{i} - 2\phi_B)]\} \quad (13)$$

where ϕ_{so}^{i} is the i'th trial value for ϕ_{so} and the initial trial value is

$$\beta\phi_{so}^{o} = 2\beta\phi_B - 2\ln\left[\beta\frac{\sqrt{(2)qN_AL_B}}{C_{ox}}\right].$$

The bulk fermi level ϕ_B is given by

$$e^{-\beta\phi_B} \equiv (n_i/N_A).$$

For the charge sheet model, comparison of (10) and (12) shows that $N(o)$ is defined by

$$qN(o) \equiv qN_AL_B\sqrt{(2)}\left\{\left[\beta\phi_{so} - 1 + \left(\frac{n_i}{N_A}\right)^2 e^{\beta\phi_{so}}\right]^{1/2} - (\beta\phi_{so} - 1)^{1/2}\right\}. \quad (14)$$

Equation (14) has been plotted in Fig. 3. It is clear from this figure that (14) has the customary $\exp(\beta\phi_{so})$ dependence in weak inversion and $\exp(\beta\phi_{so}/2)$ dependence in strong inversion. The transition occurs near the Lindner potential[14] $\beta\phi_L$ which marks the value of ϕ_{so} at which the depletion layer charge and the minority carriers make equal contributions to the field, i.e.

$$(n_i/N_A)^2 e^{\beta\phi_L} = \beta\phi_L - 1.$$

A comparison of $N(\phi_{so})$ from (14) with the usual expression

$$N_{\text{inv}} = n_i\int_o^\infty dx\,(e^{\beta\phi} - 1)\,e^{-\beta\phi_B}$$

is made in Appendix 2. It is shown that the maximum error in (14) is about 4.5% and occurs for carrier densities $<10^9/\text{cm}^2$. For carrier densities above $N(\phi_L)$ the error drops exponentially with increasing ϕ_{so}.

Now we turn to ϕ_{sL}, the potential at the drain end of the channel. In texts[8–10] and in the paper by Sah and Pao themselves[11], the assumption is made that

$$\phi_{sL} = \phi_{so} + V_D. \quad (15)$$

This assumption is natural, and in fact is demanded by a true solution of the two-dimensional Poisson equation. However, (15) ignores a constraint upon ϕ_{sL} imposed by (3), viz.

$$\beta\phi_{sL} = \beta\phi_{so} + \beta V_D + \ln\left[\frac{N(L)}{N(O)}\right] \quad (16)$$

where we adopt $\bar{\phi}_f(L) - \bar{\phi}_f(O) = V_D$. In a rigorous solution, $N(L) = N(O)$. (This is not true of the model of Refs. [5, 6] because diffusion was neglected.) However, in the gradual channel approximation

$$qN(L) = C_{ox}(V_G - \phi_{sL}) - qN_AL_B\sqrt{(2)}(\beta\phi_{sL} - 1)^{1/2} \quad (17)$$

which is *not* $qN(O)$.

A dilemma now has risen: We cannot satisfy both the condition on the quasi-fermi level at the drain and the condition on the potential! The original Pao–Sah model[7] chose to satisfy the former constraint, and has

been found to agree with experiment even in the subthreshold region[15–17]. If instead, the condition on the potential is satisfied, then agreement in the subthreshold region is lost. Therefore, we adopt the following viewpoint: The model really applies only for the source to within a depletion width or so of the drain. At this point close to, but not at the drain the potential does not satisfy (15), but the quasi-fermi level does very nearly satisfy $\bar{\phi}_f(L) - \bar{\phi}_f(O) = V_D$. From customary p-n junction theory one expects the quasi-fermi level to be close to that of the drain even in the depletion region near the drain. Thus, in deriving I–V curves we interpret the channel length "L" as differing from the metalurgical junction separation by a depletion width or so, and compute the potential at this point from (16). We envision $N(y)$ rising very rapidly near the drain to a value $N(O)$. However this region in which $N(y)$ varies rapidly is beyond that portion of the channel encompassed by the gradual channel approximation.

Given V_D and V_G, (16) and (17) determine ϕ_{sL}, the potential at the drain end of the channel. For computational purposes we have chosen a somewhat simpler route. We assume a value for ϕ_{sL} and compute the corresponding value of V_D. For the reader's convenience we plot (16) in Fig. 4 for gate voltages near threshold. This figure is the direct analogue of Fig. 4 in Barron's paper[15]. Comparison of these figures shows the close similarity between the original Pao–Sah model[7] and the charge sheet model of this paper.

We now examine the various regimes of MOSFET operation according to (11).

NON-SATURATION REGION

Figure 4 shows that for lower drain voltages the customary assumption (15) holds. Substituting (15) into (11) we obtain:

$$I = \mu^* \frac{Z}{L} C_{ox} \left\{ \left(V_G + \frac{1}{\beta} - \phi_{so} - \frac{V_D}{2} \right) V_D - \frac{(2\kappa_{sc}\epsilon_o q N_A)^{1/2}}{C_{ox}} \left[\frac{2}{3} \left(V_D + \phi_{so} - \frac{1}{\beta} \right)^{3/2} - \frac{2}{3} \left(\phi_{so} - \frac{1}{\beta} \right)^{3/2} - \frac{1}{\beta} \left(V_D + \phi_{so} - \frac{1}{\beta} \right)^{1/2} + \frac{1}{\beta} \left(\phi_{so} - \frac{1}{\beta} \right)^{1/2} \right] \right\}. \quad (18)$$

Equation (18) agrees with the usual Sah–Pao approximate formula[11] if $(1/\beta) = (kT/q)$ is neglected compared to V_G and ϕ_{so}, and if the surface potential at the source, ϕ_{so}, is replaced by $2\phi_B$ in the terms with 3/2 fractional powers. This last replacement is accurate for gate voltages well above threshold since ϕ_{so} then becomes nearly independent of V_G (see Fig. 2). In addition, under these conditions the square root terms in (18) are negligible. However, (18) becomes inaccurate for gate voltages near threshold. To illustrate this inaccuracy, I–V curves have been plotted in Fig. 5. Both (18) and the suggested procedure using (11) and (16) are presented. It is clear that if the surface potential at the source, ϕ_{so}, approaches $2\phi_B$ then (18) becomes invalid.

In computing the curves of Fig. 5 we assumed values for ϕ_{so} and ϕ_{sL} and computed I from (11), V_G from (12)

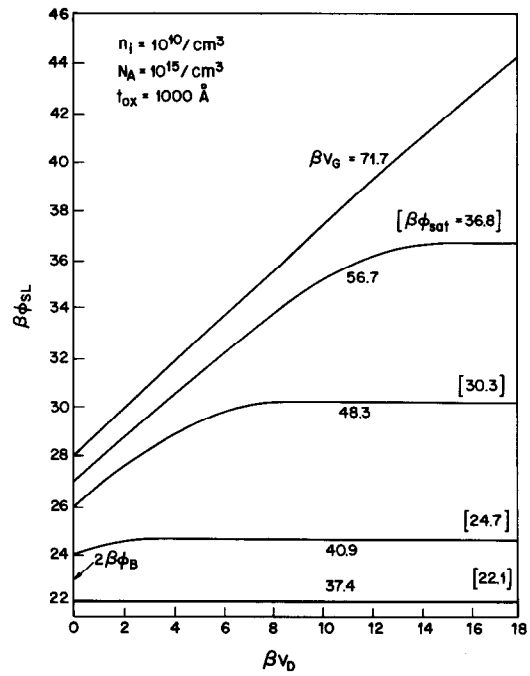

Fig. 4. A plot of potential at the drain end of the channel, ϕ_{sL}, as a function of drain voltage, V_D, in the gradual channel approximation. Gate voltages near threshold have been chosen as parameter.

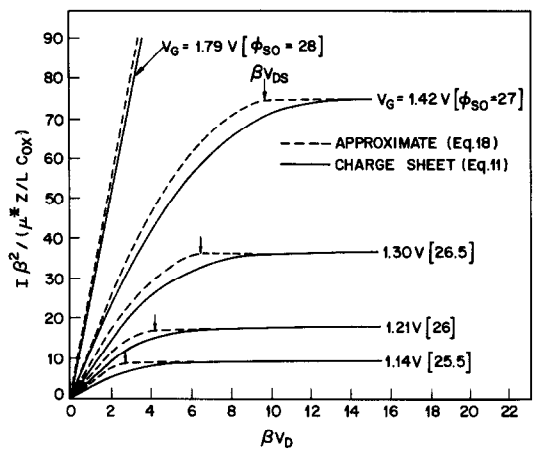

Fig. 5. Direct current vs drain voltage curves for gate voltages near threshold. The solid curves are the I–V curves of the charge sheet model which are in good agreement with the Pao–Sah model. The broken curves are the I–V curves of the approximate formula, (18). V_{DS} is the voltage at which (18) predicts I is a maximum.

and V_D from (16) in the form

$$\beta V_D = \beta(\phi_{sL} - \phi_{so}) - \ln \left\{ 1 - \frac{C_{ox}(\phi_{sL} - \phi_{so})}{qN(O)} - \frac{qN_A L_B \sqrt{2}}{qN(O)} [(\beta\phi_{sL} - 1)^{1/2} - (\beta\phi_{so} - 1)^{1/2}] \right\} \quad (19)$$

with

$$N(O) = C_{ox}(V_G - \phi_{so}) - qN_A L_B \sqrt{(2)}(\beta\phi_{so} - 1)^{1/2}.$$

In this way I–V curves can be computed very quickly using a pocket calculator.

SUBTHRESHOLD REGION

In this section we derive the form of (11) in the weak inversion region. This may seem unnecessary, since (11) applies in all bias regimes. However, in weak inversion the simpler form of (11) now to be derived allows direct comparison with earlier work in the subthreshold region[15–17].

From (3) and (10) we have

$$C_{ox}(V_G-\phi_s)=qN_AL_B\sqrt{[2(\beta\phi_s-1)]}+qN(o)\,e^{\beta(\phi_s-\phi_{so})}\,e^{-\beta(\bar{\phi}_f-\bar{\phi}_{fo})}.$$

Subtracting this relation for $y=0$ we find

$$-C_{ox}(\phi_s-\phi_{so})=qN_AL_B[\sqrt{[2(\beta\phi_s-1)]}-\sqrt{[2(\beta\phi_{so}-1)]}-qN(o)[1-e^{\beta(\phi_s-\phi_{so})}\,e^{-\beta(\bar{\phi}_f-\bar{\phi}_{fo})}]. \tag{20}$$

Consider (20) as a function of $(\phi_s-\phi_{so})$. Since $qN(o)$ is small in weak inversion compared to the depletion layer charge, (20) predicts $(\phi_s-\phi_{so})$ is small in weak inversion. Expanding (20) in powers of $(\phi_s-\phi_{so})$ we find

$$(\phi_s-\phi_{so})=\frac{qN(o)}{C_{ox}+C_D}(1-e^{-\beta(\bar{\phi}_f-\bar{\phi}_{fo})}) \tag{21}$$

where C_D is the depletion layer capacitance per unit area,

$$C_D\equiv\frac{\kappa_{sc}\epsilon_0}{L_B}\frac{1}{\sqrt{[2(\beta\phi_{so}-1)]}}. \tag{22}$$

Also, in weak inversion the inversion layer capacitance, C_{inv} is simply $\beta qN(o)$. Hence (21) can be written

$$\beta(\phi_s-\phi_{so})=\frac{C_{inv}}{C_{ox}+C_D}(1-e^{-\beta(\bar{\phi}_f-\bar{\phi}_{fo})}). \tag{23}$$

From (23) and (20) we see that $(\phi_s-\phi_{so})$ is given by (23) provided

$$\left(\frac{C_{inv}}{C_{ox}+C_D}\right)(1-e^{-\beta(\bar{\phi}_f-\bar{\phi}_{fo})})\ll 1 \tag{24}$$

and provided $\bar{\phi}_f\geq\bar{\phi}_{fo}$. These conditions are met in weak inversion.

Near the source $\bar{\phi}_f$ tends to $\bar{\phi}_{fo}$ and eqn (23) shows that ϕ_s also tends to ϕ_{so} as it should. However, as one proceeds toward the drain (23) shows that $\phi_s-\phi_{so}$ reaches a maximum value $C_{inv}/[\beta(C_{ox}+C_D)]$ which is independent of V_D for $V_D\gg\beta^{-1}$. That is, the condition $\phi_s(L)=\phi_{so}+V_D$ cannot be satisfied. This behavior is consistent with our earlier discussion of Fig. 4. In addition, because ϕ_{sat} is so close to ϕ_{so} in weak inversion [$\beta\phi_{sat}-\beta\phi_{so}\approx C_{inv}/(C_{ox}+C_D)$, $\phi_s(y)$ is almost y-independent in weak inversion as pointed out by Barron[15] on the basis of the Pao–Sah model. Further discussion may be found in Appendix 3.

Using (23) in (11) and expanding (11) in powers of $(\phi_s-\phi_{so})$ we find for $y=L$

$$I=\mu^*q\left(\frac{Z}{L}\right)\frac{1}{\beta}N(o)(1-e^{-\beta V_D}) \tag{25}$$

where we have $\bar{\phi}_f(L)-\bar{\phi}_f(o)=V_D$, the drain voltage. This is the same as the result for the subthreshold current using the Pao–Sah model[15–17]. It should be noted that the square root terms in (11) are necessary for success in the weak inversion regime. These terms are not present in the approximate Sah–Pao formula[11]. An explicit formula for the gate-voltage dependence of (25) is derived in Appendix 3.

It is clear that the analysis does not really apply out to $y=L$ since $\phi_s(L)\neq V_D+\phi_{so}$. Hence the channel length in (25) must be considered accurate only to within a drain depletion width or so of the true metalurgical source-drain separation. In the same way, V_D is only approximately the drain voltage, since instead of V_D the quasi fermi level separation, $\bar{\phi}_f-\bar{\phi}_{fo}$, evaluated somewhere short of $y=L$ should be taken.

SATURATION REGION

In this section we shall discuss first the failings of the usual approximate treatment of saturation found in most textbooks. Equation (11) can be solved for ϕ_s as a function of y or, more correctly, as a function of $\zeta\equiv Iy/(kT\mu^*ZC_{ox})$. In Fig. 6 a plot of $\phi_s(y)$ from eqn (11) is shown for two choices of gate voltage, V_G. Figure 6 can be used to determine the current, I, for any drain voltage, V_D. Suppose one assumes $\phi_s(L)=V_D+\phi_{so}$. (This assumption is not always valid, as Fig. 4 shows. However,

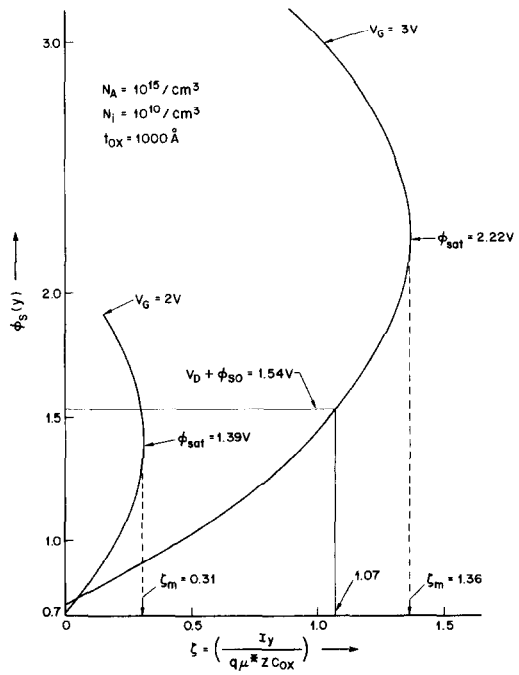

Fig. 6. The surface potential, $\phi_s(y)$, as a function of distance, $\zeta=Iy/kT\mu^*ZC_{ox}$. Equation (11) has been used with $N_A=10^{15}/cm^3$, and an oxide thickness of 1000 Å. The straight lines illustrate the determination of I for a given V_D under the approximate condition $\phi_{sL}=\phi_{so}+V_D$ (eqn 15).

this is the usual textbook assumption.) Then for any choice of V_D one can find the corresponding value of ζ from the curve in Fig. 6 for the appropriate gate voltage. For example for $V_D = 0.8$ V and $V_G = 3$ V, $\phi_{so} + V_D = 1.54$ and Fig. 6 shows

$$\zeta = \left(\frac{IL}{q\mu^* C_{ox}}\right) = 1.07 \text{ V}^2/\text{Coulomb}.$$

Hence I is determined if the various device parameters are known. This graphical procedure is entirely equivalent to using the approximate result (18).

A complication in this procedure arises if $\phi_{so} + V_D$ is greater than the knee in the curves of Fig. 6. This knee occurs at a value of potential, ϕ_{sat}, determined by the pinch-off condition.

$$C_{ox}(V_G - \phi_{\text{sat}}) = \sqrt{(2)qN_A L_B(\beta\phi_{\text{sat}} - 1)^{1/2}}. \quad (26)$$

At this point the inversion layer carrier density goes to zero. This condition can be found by equating $(dy/d\phi_s)$ to zero, after differentiating eqn (11). If we define V_{DS} by

$$\phi_{so} + V_{DS} \equiv \phi_{\text{sat}} \quad (27)$$

then eqn (26) is identical to that used to obtain the saturation drain voltage in the approximate Sah–Pao formula[11]. (See eqn (A3.1) in Appendix 3).

In the event $V_D > V_{DS}$, Fig. 6 fails to give the potential in the portion of the channel where $\phi_s(y) > \phi_{\text{sat}}$. Instead the curves of Fig. 6 bend back in an unphysical manner. In addition, for $\phi_s > \phi_{\text{sat}}$ the channel carrier density must go negative to satisfy eqn (10). In short, the calculation goes to pieces for $V_D > V_{DS}$.

If (18) is used instead of the above graphical approach, then the corresponding failure is that the current reaches a maximum for $V_D = V_{DS}$, and then begins to *decrease* for $V_D > V_{DS}$. The customary procedure taken with the approximate formula (18) is to *assume* that for $V_D > V_{DS}$ the potential at the drain end of the channel simply remains pinned at $\phi_s(L) = \phi_{\text{sat}}$, so that the potential is no longer affected by the drain voltage for $V_D > V_{DS}$. This in turn means that the current simply saturates at a value I_{DS} given by (18) for $V_D = V_{DS}$. This procedure was used to obtain the dashed-line curves in Fig. 5.

We now wish to show that this entire problem need never arise. Examination of Fig. (4) shows that in fact for larger values of V_D the surface potential ceases to increase and saturates at a value ϕ_{sat} which is the same as ϕ_{sat} of (26). (This can be verified using (16); as $N(L) \to 0$, $V_D \to \infty$ as $\phi_{sL} \to \phi_{\text{sat}}$.) Consequently only the physically meaningful region of the curves in Fig. 6 is needed in finding the current or the dependence of potential on distance. The pinch-off condition is reached only asymptotically as $V_D \to \infty$ because, according to Fig. 4, $\phi_{sL} \to \phi_{\text{sat}}$ asymptotically as $V_D \to \infty$. This behavior of ϕ_{sL} in turn means that the drain conductance, g_d

$$g_d \equiv \left(\frac{\partial I}{\partial V_D}\right)_{V_G}$$

vanishes only asymptotically.

In Fig. 7, g_d is plotted as a function of drain voltage and compared with the textbook or approximate Sah–Pao formula based upon (18). The asymptotic approach of g_d to zero is evident. The failure of the approximate formula for low gate voltages is also evident. Figure 7 also illustrates that g_d approaches the correct weak inversion limit as V_G approaches threshold.

Using (11) g_d is found to be

$$g_d = \mu^* q \frac{Z}{L} N(L)$$

$$= \mu^* q \frac{Z}{L} N(O) \times \left\{\frac{C_{ox}(V_G - \phi_{sL}) - \sqrt{(2)qN_A L_B(\beta\phi_{sL} - 1)^{1/2}}}{C_{ox}(V_G - \phi_{so}) - \sqrt{(2)qN_A L_B(\beta\phi_{so} - 1)^{1/2}}}\right\}. \quad (28)$$

The weak inversion limit is, from (28) or from (25)

$$g_d = \mu^* q \frac{Z}{L} N(O)\, e^{-\beta V_D} \quad (29)$$

and is also shown in Fig. 7. It may be noted from Fig. 7 or (29) that a small-signal measurement of g_d in weak inversion requires an extremely small-amplitude a.c. drain voltage because of the exponential drop of g_d with V_D. Most weak inversion measurements have not satisfied this constraint.

A similar comparison of the transconductance, g_m

$$g_m \equiv \left(\frac{\partial I}{\partial V_G}\right)_{V_D}$$

is made in Fig. 8. Here, apart from a very small correction (11) predicts

$$g_m = \mu^* \frac{Z}{L} C_{ox}(\phi_{sL} - \phi_{so}). \quad (30)$$

This would agree with the usual approximate formula if (15) were valid. However, we use (16) in the form (19). This results in a smoothly varying g_m which saturates only asymptotically as $V_D \to \infty$. Again, at larger gate voltages the descrepancy between (30) and the usual approximation is small. However, in the near threshold

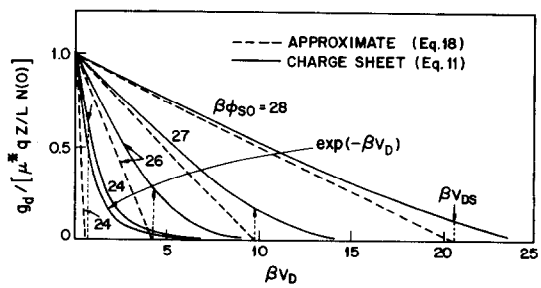

Fig. 7. Drain conductance g_d vs drain voltage, V_D. The solid line is the charge-sheet model result. The broken line is the usual textbook result which vanishes at $V_D = V_{DS}$, the saturation voltage. Also shown is the weak inversion limit, $\exp(-\beta V_D)$, predicted by both the charge-sheet model and the Pao–Sah model.

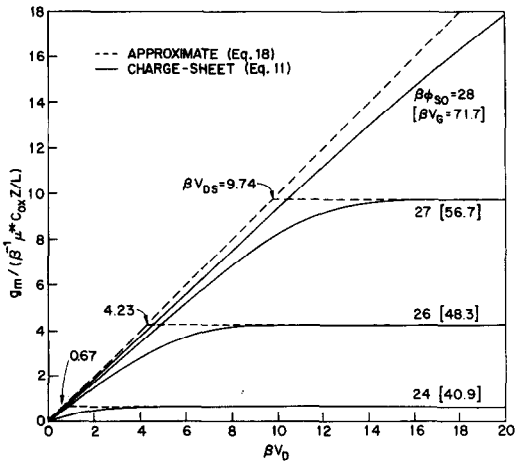

Fig. 8. The transconductance, g_m, vs drain voltage. Again the solid line curve is the charge sheet model result and the broken-line curve is the textbook result.

region (30) is very different and approaches the correct weak inversion limit.

CONCLUSION

It has been shown that the direct-current vs voltage curves of long channel MOSFETs are given just as well by a charge sheet model as by the original Pao–Sah model[7]. This is true in all regimes of operation, including the subthreshold regime and the saturation regime. The only differences are small corrections in gate voltage or surface potential of $(kT/q) \simeq 25$ mV.

The analysis has led to simple formulas for the current and small signal parameters. These formulas are similar to the approximate formulas introduced by Sah and Pao[11] and used in texts[8–10] in the non-saturation regime for large gate voltages. However, unlike these approximate formulas, the formulas of this charge sheet model remain valid in the subthreshold region, retaining agreement with the original Pao–Sah integral formulation[7]. In common with the Pao–Sah model, formulas of the charge sheet model provide a natural treatment of saturation. The small signal parameters vary smoothly with drain voltage, approaching their saturation limits only asymptotically. No arbitrary assumptions are needed to continue the formulas beyond pinch-off, becaused pinch-off never is attained.

In general the terms "drain voltage", "channel length" etc. are only approximate terms in both the charge sheet model and the Pao–Sah model when the gradual channel approximation has been used. They must be obtained experimentally by fitting measured I–V curves.

The close correspondence between the two models suggests that the shape of the inversion layer and the details of the minority carrier distribution within the inversion layer are only very minor influences upon the I–V curves. If the details of the inversion layer remain small effects for short-channel devices, then the charge sheet model will work well with a two-dimensional Poisson equation using eqns (4)–(6). With a two-dimensional Poisson equation the gradual channel approximation can be abandoned. As a result both the boundary condition upon the quasi-fermi level and that upon the potential can be satisfied at the drain. The work of Loeb *et al.*[5] indicates such a short-channel model will be successful in the region well above threshold. The correct weak inversion behavior demonstrated by our model which includes diffusion raises the hope for short channels that weak inversion also will be accessible in this manner.

Acknowledgements—The author wishes to thank D. Kahng, K. K. Thornber, and H. K. Gummel for helpful comments and discussions.

REFERENCES

1. M. Heydemann, *L'Onde Electronique* **52**, 185 (1972).
2. D. Vandorpe, J. Borel, G. Merckel and P. Saintot, *Solid-St. Electron.* **15**, 547 (1972).
3. D. P. Kennedy and P. C. Murley, *IBM J. Res. and Develop.* **17**, 2 (1973).
4. J. A. Guerst, *Solid-St. Electron.* **9**, 129 (1966).
5. H. W. Loeb, R. Andrew and W. Love, *Electron. Lett.* **4**, 352 (1968).
6. G. A. Armstrong, J. A. Magowan and W. D. Ryan, *Electron. Lett* **5**, 406 (1969).
7. H. C. Pao and C. T. Sah, *Solid-St. Electron.* **9**, 927 (1966).
8. A. S. Grove, *Physics and Technology of Semiconductor Devices.* Wiley, New York (1967).
9. R. S. C. Cobbold, *Theory and Applications of Field Effect Transistors.* Wiley, New York (1970).
10. S. M. Sze, *Physics of Semiconductor Devices.* Wiley, New York (1969).
11. C. T. Sah and H. C. Pao, *IEEE Trans. Electron Dev.* **ED-13**, 393 (1966).
12. H. K. J. Ihantola and J. L. Moll, *Solid-St. Electron.* **7**, 423 (1964).
13. D. Kahng, Bell Laboratories Memorandum dated Jan. 16, 1961 (unpublished). Copies are available from D. Kahng.
14. R. Lindner, *Bell Syst. Tech. J.* **41**, 803 (1962).
15. M. B. Barron, *Solid-St. Electron.* **15**, 293 (1972).
16. R. M. Swanson and J. E. Meindl, *IEEE J. of Solid-St. Circuits*, **SC-7**, 146 (1972).
17. R. R. Troutman and S. N. Chakravarti, *IEEE Trans. Circuit Theory* **CT-20**, 659 (1973).
18. F. de la Moneda, *IEEE Trans. Circuit Theory* **CT-20**, 666 (1973).

APPENDIX 1

General dependence of current on quasi-fermi level gradient

In this Appendix we wish to show that the relation

$$I = -qZN(y)\mu^* \frac{d\tilde{\phi}_f(y)}{dy} \tag{A1.1}$$

is sufficiently general to include two-dimensional current flows. To do this we assume a quasi-fermi level approximation and take the current density to be

$$\mathbf{j} = -q\mu(n - n_f)\nabla\phi_f \tag{A1.2}$$

where $(n - n_f)$ is the minority carrier density per unit volume in excess of the zero band-banding density, n_f:

$$n_f = n_i \exp(-\beta\phi_f). \tag{A1.3}$$

We define the total device current to be

$$I = Z\int_o^\infty dx j_y(x, y) \tag{A1.4}$$

where the coordinate system of Fig. 1 is used. Then using (A1.2)

$$I = -qZN(y)\left\langle \mu \frac{\partial \phi_f}{\partial y} \right\rangle \tag{A1.5}$$

where the local excess carrier density, $N(y)$ is defined by

$$N(y) \equiv \int_o^\infty dx[n(x, y) - n_f(x, y)] \tag{A1.6}$$

and the average mobility—ϕ_f gradient product across the inversion layer is defined as

$$\left\langle \mu \frac{\partial \phi_f}{\partial y} \right\rangle \equiv \frac{1}{N(y)} \int_o^\infty dx[n(x, y) - n_f(x, y)]\, \mu \frac{\partial \phi_f(x, y)}{\partial y}. \tag{A1.7}$$

The term "average" for (A1.7) is appropriate in the sense that $(n - n_f)$ is the weighting function of the average, and division by $N(y)$ insures that the average of a constant is the constant itself.

Since $\langle \mu(\partial \phi_f/\partial y) \rangle$ is merely some function of y alone, we are free to define some function $\bar{\phi}_f(y)$, and some "effective" mobility, μ^*, such that

$$\left\langle \mu \frac{\partial \phi_f}{\partial y} \right\rangle \equiv \mu^* \frac{d\bar{\phi}_f}{dy}. \tag{A1.8}$$

The relation between μ^* and the microscopic mobility, μ, is not direct, and may account for difficulties in trying to make theoretical calculations of μ fit experimental determinations of μ^*. Using (A1.8), the current from (A1.5) becomes

$$I = -q\mu^* Z N(y) \frac{d\bar{\phi}_f}{dy}. \tag{A1.9}$$

To further pin down the meaning of $\bar{\sigma}_f$ and μ^*, we might consider calculating $N(y)$, (A1.6). If we assume a Boltzmann gas, (A1.6) becomes

$$N(y) = n_i \int_o^\infty dx\, e^{-\beta\phi_f(x,y)} [e^{\beta\phi(x,y)} - 1] \tag{A1.10}$$

where $\phi(x, y)$ is the electrostatic potential and $\phi_f(x, y)$ is the microscopic quasi-fermi level. A commonly used and very successful approximation of (A1.10) results if we assume $\phi_f(x, y)$ is not very different from $\bar{\phi}_f(y)$[18]. then expanding (A1.10) in powers of $(\phi_f - \bar{\phi}_f)$ and retaining the leading term we find:

$$N(y) \simeq n_i\, e^{-\beta\bar{\phi}_f(y)} \int_o^\infty dx\, (e^{\beta\phi(x,y)} - 1). \tag{A1.11}$$

The first neglected term is $\beta - \bar{\phi}_f\rangle_0$ where

$$\beta\langle\phi_f - \bar{\phi}_f\rangle_0 \equiv \int_o^\infty dx\, [e^{\beta\phi(x,y)} - 1][\phi_f(x, y) - \bar{\phi}_f(y)] \Big/ \int_o^\infty dx\, [e^{\beta\phi(x,y)} - 1]. \tag{A1.12}$$

We may then remove some of the uncertainty in $\bar{\phi}_f(y)$ by requiring this neglected term to vanish. This requirement can always be met if one is willing to allow μ^* to vary with y. Then (A1.8) and the requirement that (A1.12) vanish define $\bar{\phi}_f$ and μ^* unambigiously. If μ^* is not to vary with y, then one could invent criteria other than the vanishing of (A1.12). For example, one could require that the average of (A1.12) over the length of the channel vanish. Whatever constraint one chooses (A1.1) is then established with no constraints on the dimensionality of the current flow.

APPENDIX 2

In this appendix we compare the charge-sheet model estimate of $N(o)$ which is

$$N(o) = N_A L_B \sqrt{(2)} \left\{ \left[\beta\phi_{so} - 1 + \left(\frac{n_i}{N_A}\right)^2 e^{\beta\phi_{so}} \right]^{1/2} - [\beta\phi_{so} - 1]^{1/2} \right\} \tag{A2.1}$$

with the more usual estimate of MOS capacitor theory, N_{inv}, given by

$$N_{inv} = n_i \int_o^\infty dx\, [e^{\beta\phi(x)} - 1]\, e^{-\beta\phi_B} \tag{A2.2}$$

where $\phi(x)$ is the potential from the one-dimensional Poisson equation. Changing variables from x to $\phi(x)$ (A2.2) becomes

$$N_{inv}(\phi_{so}) = n_i \int_o^{\phi_{so}} d\phi\, \frac{(e^{\beta\phi} - 1)}{(d\phi/dx)}\, e^{-\beta\phi_B} \tag{A2.3}$$

where

$$\frac{d\phi}{dx} = \frac{\sqrt{(2)} q N_A L_B}{\kappa_{sc}\epsilon_o} \left[e^{-\beta\phi} + \beta\phi - 1 + \left(\frac{n_i}{N_A}\right)^2 (e^{\beta\phi} - \beta\phi + 1) \right]^{1/2}. \tag{A2.4}$$

Rather than take a numerical integration of (A2.3) and compare this with (A2.1), we compare the derivatives of these two expressions with respect to ϕ_{so}. This provides a simple error analysis of the minority carrier capacitance. This error analysis is easily extended to determine the error in $N(o)$.

Differentiating (A2.1) with respect to ϕ_{so} we find

$$C_{min} \equiv \frac{d}{d\phi_{so}} [qN(o)] = C_{SC} - C_D \tag{A2.5}$$

where C_{SC} is the usual semiconductor capacitance in depletion or inversion [e.g. see Ref. [10], p. 432, eqn (20)]:

$$C_{SC} = C_{FB} \frac{1 + \left(\frac{n_i}{N_A}\right)^2 e^{\beta\phi_{so}}}{\sqrt{(2)} \left[\beta\phi_{so} - 1 + \left(\frac{n_i}{N_A}\right)^2 e^{\beta\phi_{so}} \right]^{1/2}} \tag{A2.6}$$

with $C_{FB} = \kappa_{sc}\epsilon_o/L_B$. The capacitance C_D is the depletion layer capacitance:

$$C_D = C_{FB} \frac{1}{\sqrt{(2)}(\beta\phi_{so} - 1)^{1/2}}. \tag{A2.7}$$

On the other hand, differentiation of (A2.3) provides

$$C_{inv} \equiv \frac{d}{d\phi_{so}} qN_{inv} \simeq C_{FB} \frac{\left(\frac{n_i}{N_A}\right)^2 e^{\beta\phi_{so}}}{\sqrt{(2)} \left[\beta\phi_{so} - 1 + \left(\frac{n_i}{N_A}\right)^2 e^{\beta\phi_{so}} \right]^{1/2}}. \tag{A2.8}$$

In (A2.8) the approximation $e^{\beta\phi_{so}} \gg (\beta\phi_{so} - 1)$ has been made, which introduces negligible error in the weak inversion range of $\beta\phi_{so}$ or for larger $\beta\phi_{so}$. Typically $\beta\phi_{so} \geq 20$.

Comparison of (A2.5) and (A2.8) indicates the relative error in capacitance, ϵ, is:

$$\epsilon \equiv \frac{C_{inv} - C_{min}}{C_{inv}} \simeq e^{-\beta\phi_{so}} \left(\frac{N_A}{n_i}\right)^2 \left\{ \left[1 + \left(\frac{n_i}{N_A}\right)^2 \frac{e^{\beta\phi_{so}}}{\beta\phi_{so} - 1} \right]^{1/2} - 1 \right\}. \tag{A2.9}$$

This error is plotted in Fig. 9 for various doping levels. The worst case error occurs for small $\beta\phi_{so}$ and is bounded by

$$\left(\frac{C_{inv} - C_{min}}{C_{inv}}\right) \leq \frac{1}{2(\beta\phi_{so} - 1)} = \epsilon_{max} \tag{A2.10}$$

as is found from (A2.9) by expanding the square root for $(n_i/N_A)^2 \exp \beta\phi_{so} < 1$. This maximum error is also shown in Fig. 9.

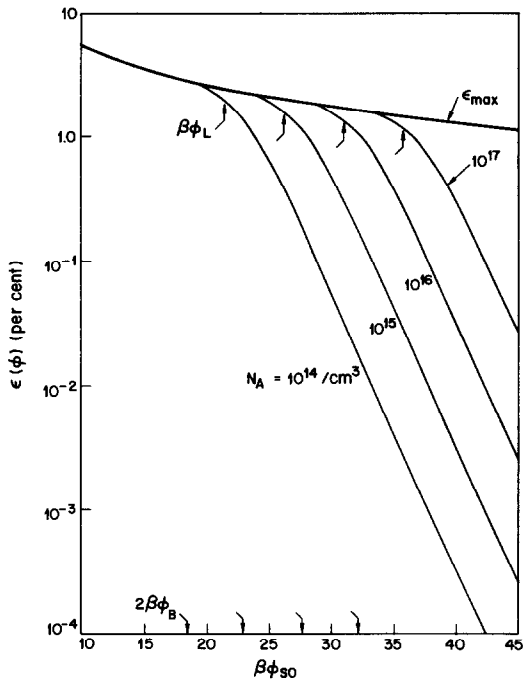

Fig. 9. The relative error in the minority carrier capacitance near the source in the charge sheet model. The heavy line shows the worst case error which occurs in weak inversion.

The error in $N(0)$ can be estimated from ϵ since

$$\frac{N_{inv}-N(0)}{N_{inv}}=\frac{1}{qN_{inv}}\int_{\phi_B}^{\phi_{so}}d\phi\,\epsilon(\phi)C_{inv}(\phi)$$
$$=\frac{C_{FB}}{\sqrt{(2)}qN_{inv}}\int_{\phi_B}^{\phi_{so}}d\phi\left(\left[1+\left(\frac{n_i}{N_A}\right)^2\frac{e^{\beta\phi}}{\beta\phi-1}\right]^{1/2}-1\right)\Big/$$
$$\left\{(\beta\phi-1)^{1/2}\left[1+\left(\frac{n_i}{N_A}\right)^2\frac{e^{\beta\phi}}{\beta\phi-1}\right]^{1/2}\right\}. \qquad (A2.11)$$

In weak inversion the error in the integrand is worst, as Fig. 9 shows. But in this case (A2.11) shows the error in $N(O)$ is:

$$\frac{N_{inv}-N(O)}{N_{inv}}\leq\frac{1}{qN_{inv}}\int_{\phi_B}^{\phi_{so}}d\phi\,\epsilon_{max}(\phi)C_{inv}(\phi)$$
$$\leq\frac{C_{FB}}{\sqrt{(2)}qN_{inv}}\int_{\phi_B}^{\phi_{so}}d\phi\,\frac{1}{2(\beta\phi-1)}\left(\frac{n_i}{N_A}\right)^2\frac{e^{\beta\phi}}{(\beta\phi-1)^{1/2}}$$
$$=\frac{C_{FB}}{2\sqrt{(2)}\beta qN_{inv}}\left(\frac{n_i}{N_A}\right)^2\left\{\frac{e^{\beta\phi_{so}}}{(\beta\phi_{so}-1)^{3/2}}-\frac{e^{\beta\phi_B}}{(\beta\phi_B-1)^{3/2}}\right.$$
$$\left.+\frac{3}{2}\beta\int_{\phi_B}^{\phi_{so}}\frac{e^{\beta\phi}}{(\beta\phi-1)^{5/2}}d\phi\right\}.$$

Using the weak inversion result $C_{inv}=\beta qN_{inv}$ we find

$$\frac{N_{inv}-N(O)}{N_{inv}}\leq\frac{1}{2}\left\{\frac{1}{(\beta\phi_{so}-1)}-e^{-\beta(\phi_{so}-\phi_B)}\frac{(\beta\phi_{so}-1)^{1/2}}{(\beta\phi_B-1)^{3/2}}\right.$$
$$\left.+\frac{3}{2}[1-e^{-\beta(\phi_{so}-\phi_B)}]\frac{(\beta\phi_{so}-1)^{1/2}}{(\beta\phi_B-1)^{5/2}}\right\}. \qquad (A2.12)$$

This error is considerably less than the maximum error in the integrand. To estimate the error take $\beta\phi_{so}=2\beta\phi_B$, the maximum surface potential in the weak inversion range. Then the error bound for weak inversion from (A2.12) is

$$\frac{N_{inv}-N(O)}{N_{inv}}\leq\frac{1}{2}\left\{\frac{1}{(2\beta\phi_B-1)}+\frac{3}{2}\frac{(2\beta\phi_B-1)^{1/2}}{(\beta\phi_B-1)^{5/2}}\right\}. \qquad (A2.13)$$

For $N_A=10^{14}$/cm^3 this bound is 4.5%, for $N_A=10^{17}$/cm^2 it is 2.1%. In strong inversion the error will be less because the error in Fig. 9 drops exponentially, and this small error region is the region which contributes most strongly to N_{inv}.

APPENDIX 3

Further discussion of the subthreshold region

In this Appendix an explicit form for the gate voltage dependence of the subthreshold current, (25), is derived. this expression then is compared with (11) of the text.

As Fig. 4 of the text shows, if the gate voltage is reduced, then the saturation value of surface potential, ϕ_{sat}, becomes closer and closer to the value of the potential at the source, ϕ_{so}. From (26), $\beta\phi_{sat}$ is given by:

$$\beta\phi_{sat}=\beta V_G-\frac{a^2}{2}\left\{\left[1+\frac{4}{a^2}(\beta V_G-1)\right]^{1/2}-1\right\} \qquad (A3.1)$$

where $a=(\kappa_{sc}/\kappa_{ox})(t_{ox}/L_B)\sqrt{(2)}$. This relation is plotted in Fig. 10 for the case $N_A=10^{15}$/cm^3, $n_i=10^{10}$/cm^3, $t_{ox}=1000$ Å. From Fig. 10 it can be seen that for $\beta\phi_{so}<2\beta\phi_B$ the approximation $\beta\phi_{so}\approx\beta\phi_{sat}$ is valid. This makes it possible to use (A3.1) to obtain the explicit gate voltage dependence of the subthreshold current.

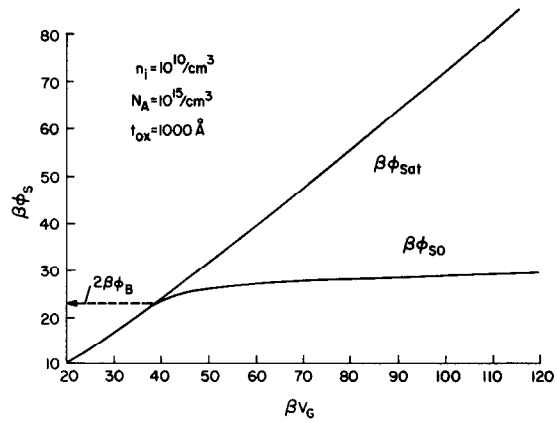

Fig. 10. A comparison of ϕ_{sat} and ϕ_{so} as functions of gate voltage, V_G. In the regime where the surface potential at the source, ϕ_{so}, is less than $2\phi_B$ the approximation $\phi_{sat}\simeq\phi_{so}$ is valid.

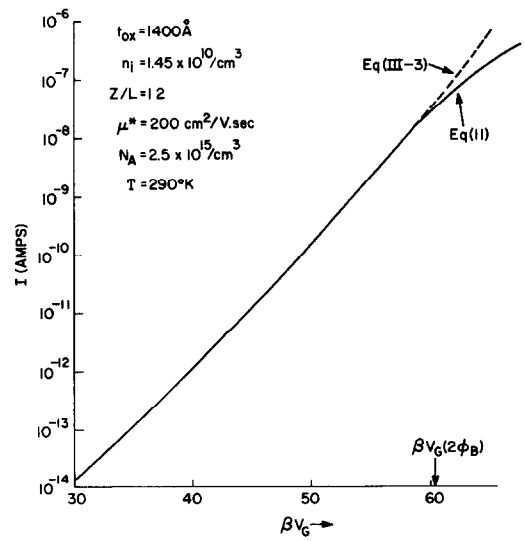

Fig. 11. Subthreshold current, I, vs gate voltage, V_G. For the region $\phi_{sat}<2\phi_B$ eqn (A3.3) provides a good approximation to the more accurate (11) of the text.

To do this we expand (14) for $qN(o)$ assuming $\exp(\beta\phi_{so} - 2\beta\phi_B) \ll (\beta\phi_{so} - 1)^{1/2}$. The result is

$$qN(o) \simeq \left(\frac{aC_{ox}}{2\beta}\right)\left(\frac{n_i}{N_A}\right)^2 \frac{e^{\beta\phi_{so}}}{(\beta\phi_{so} - 1)^{1/2}}. \quad \text{(A3.2)}$$

Then using (25) and the assumption $\beta\phi_{so} \approx \beta\phi_{sat}$ the current becomes

$$I = \mu^*\left(\frac{Z}{L}\right)\frac{aC_{ox}}{2\beta^2}\left(\frac{n_i}{N_A}\right)^2 (1 - e^{-\beta V_D})\, e^{\beta\phi_{sat}}(\beta\phi_{sat} - 1)^{-1/2} \quad \text{(A3.3)}$$

where $\beta\phi_{sat}$ is a known function of βV_G from (A3.1). Equation (A3.3) agrees with Barron's eqn (25)[15]. However, Barron did not recognize $\beta\phi_{so} \approx \beta\phi_{sat}$ and therefore did not obtain an explicit form for the gate voltage dependence of the subthreshold current. Comparison of (A3.3) and the more general (11) from the text is made in Fig. 11 where (11) has been used under the assumption $\phi_{sL} = \phi_{sat}$, which is valid for even minute drain voltages $[\beta V_D \geq C_{inv}/(C_{ox} + C_D)]$ in the subthreshold region. Figure 11 shows that (A3.3) is very accurate in the region of gate voltages corresponding to $\phi_{so} < 2\phi_B$. For $\phi_{so} \geq 2\phi_B$, the full (11) is needed.

The parameters for the calculation in Fig. 11 are chosen to agree with those of Barron[15] viz. $t_{ox} = 1400$ Å, $n_i = 1.45 \times 10^{10}/\text{cm}^2$, $Z/L = 12$ $\mu^* = 200\ \text{cm}^2/\text{V sec}$ and $N_A = 2.5 \times 10^{15}/\text{cm}^3$. Our Fig. 11 agrees with the theoretical curve of Barron's Fig. 11(a) based upon numerical calculation using the full Pao–Sah double-integral formula.